A New Boundary Element Method for Accurate Modeling of Lossy Substrates with Arbitrary Doping Profiles*

Xiren Wang, Wenjian Yu, and Zeyi Wang

Eda Lab, Dept. Computer Science & Technology,
Tsinghua Univ., Beijing, 100084, China

Abstract - It is important to model substrate couplings for SoC/mixed-signal circuit designs. After introducing the continuation equation of full current in lossy substrates, we present a new direct boundary element method (DBEM), which can handle the substrates with arbitrary doping profiles. Three techniques can speed up the DBEM remarkably, which include reusing coefficient matrices for multiple-frequency calculation, condensing the linear system, and sparsifying coefficient matrix. Numerical experiments illustrate that DBEM has high accuracy and high efficiency, and is versatile for arbitrary doping profiles.

I Introduction

There are currently increasing demands for high-integration circuits [1]. High-speed digital components and highly-sensitive analog components are often built on a common substrate. Although the high integration has some advantages, such as low power dissipation [2], there is a problem that the current noises injected by digital components travel the shared substrate and impact sensitive analog components severely [3]. Besides, substrate losses also impact circuit performances considerably. For instance, the quality factor of such passive devices as inductors is important for circuit performances, especially in wireless communication applications. But it is limited by substrate losses, especially at high frequencies. Thus acknowledge of lossy substrates is very important even critical for designs [4].

A resistance network model of a substrate is often efficient at frequency of up to several gigahertz. Some numerical methods are presented for the resistive simulation, including finite element method (FEM), finite difference method (FDM) [5], and methods based on Green's function (sometimes also called boundary element method) [2, 4, 6, 7]. FEM and FDM are too slow, since they discretize entire volume of a substrate. However, they have the advantage of versatility, i.e., they can handle substrates with arbitrary doping profiles rather than only layered substrates.

The Green's function based methods [2, 6, 7] are generally faster than FDM and FEM, because they only discretize contact surfaces. A suitable Green's function that satisfies boundary conditions needs to be found. For multilayered substrates, the function consists of multiple infinite series, and converges slowly. In [4], a 'numerically stable' method was proposed to calculate the Green's function with the acceleration of discrete cosine transform (DCT) [7]. However, it is not actually stable, with further remedy presented in [8]. In [2], there is an excellent idea of eigendecomposition, which results in a speedup of a dozen over the above DCT-Green's function method. The coefficient matrix is dense for these methods, however. Storing and solving the linear system are memory- and time-consuming.

On the other hand, the resistive model becomes invalid at high frequencies, and a comprehensive frequency-dependent impedance model is desired. The method in [4] is able to give such impedances. However, it also needs to find an expensive Green's function, whose derivation is based on the layered structure of substrates.

Note that substrates are not always stratified. In fact, there are lots of realistic substrates with layout-dependent doping profiles, such as oxide wells, trenches, sinkers, buried diffusions and etc [9]. There are also special structures like Faraday shields and junction shields [10] for noise reduction. To simulate such substrates, the methods based on Green's function meet much difficulty.

In this paper, we bring forward a direct boundary element method (DBEM) [3, 11, 12] for lossy substrate modeling. Conventionally it is applied in electrostatic DC capacitance extraction [12] or resistance extraction [11]. We will modify it to model lossy substrates at any frequency with the help of the concept of complex permittivity [13].

In DBEM, only substrate boundary is discretized, then the variables are fewer than in FDM/FEM. Only the free-space Green's function is used, which brings two advantages. One is that no derivation of the function is needed, and its computation is also straightforward. The other is that the function is independent of structures, so DBEM can handle substrates with arbitrary doping profiles. Besides, three kinds of accelerating techniques are presented, which are reusing coefficient matrices for multiple-frequency calculation, condensing the linear system before solving, and sparsifying the coefficient matrix. They can enhance the efficiency of DBEM considerably, but preserve the accuracy exactly.

The rest is organized as follows. In Section II, DBEM principle for impedance modeling is presented. In Section III, the accelerations for DBEM are described separately. Numerical experiments follows, so as to demonstrate the accuracy and efficiency of the method. A special case is a non-stratified substrate with lateral resistivity variation, and it can illustrate versatility of the method. The conclusions are given at last.

* This work is supported by the China National Science Foundation under Grant 60401010. It is also partly supported by National High Technology Research and Development Program of China (No. 2004AA1Z1050).

0-7803-9451-8/06/$20.00 ©2006 IEEE.

II. Frequency-Dependent Extraction of Substrate Coupling with DBEM

Fig. 1 shows an example of lossy substrate, which is constituted by layers of mediums M_i (with finite resistivity) and contacts C_j. There is usually a grounded plane on the bottom. In many cases, contacts are assumed to be on the top. Here, however, they can be placed anywhere if necessary.

For lossy substrates (such as Silicon), the coupling between contacts can be modeled as frequency-dependent impedances. To get the impedances needs to pre-set voltages of contacts, and then to calculate the full current flowing through contacts. The reciprocal of the current is related to the desired impedance.

Assume electric potential of contacts to be in $u = \overline{u}e^{j\omega t}$ form, where $\overline{u}$ is the maximum voltage, ω is the angular frequency, and t is time. Electric field within the substrate is also in $E = \overline{E}e^{j\omega t+\theta}$ form. Start from the Maxwell equation

$$\nabla \times H = J + \frac{\partial D}{\partial t}, \tag{1}$$

where H is the magnetic filed intensity, J is the conductance (ohmic) current density, D is the electric displacement. For mediums with constant conductivity σ and permittivity ε,

$$(\sigma + j\omega\varepsilon)\nabla \cdot E = 0. \tag{2}$$

Because $E = -\nabla u$ [1], the following Laplace equation holds:

$$\nabla^2 u = 0, \qquad \text{in medium } M_i \tag{3}$$

with the mixed boundary conditions of

$$u = \overline{u}, \text{ on contact surfaces (Dirichlet boundary)} \tag{4a}$$
$$E_n = 0, \text{ on natural boundary (Neumann boundary)} \tag{4b}$$

where $\overline{u}$ is pre-set voltage of contacts, usually 1V or 0V. E_n is normal electric field intensity. Besides, the potential and full current is continuous on the interface of adjacent mediums a and b:

$$u_a = u_b, \tag{5a}$$
$$(\sigma_a + j\omega\varepsilon_a)E_{n,a} = (\sigma_b + j\omega\varepsilon_b)E_{n,b}. \tag{5b}$$

where σ_a and σ_b (ε_a and ε_b) are the conductivity (permittivity) of regions a and b, respectively.

[1]Generally speaking, $E = -\nabla u - \frac{\partial A}{\partial t}$, where A is the magnetic vector potential. Here we adopt the Coulomb Gauge [15], which defines $\nabla \cdot A = 0$. Thus $E = -\nabla u$.

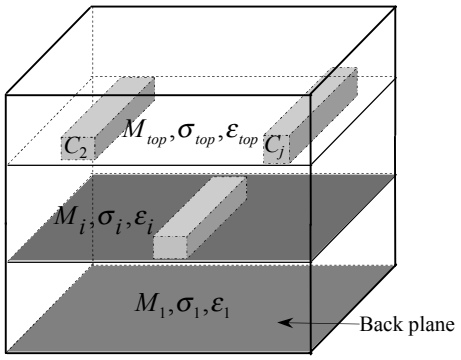

Fig. 1 An example substrate with a back plane. The non-zero conductivity of medium M_i is σ_i, and the permittivity is ε_i.

If E_n is known, we can get the current between contacts m and k. If the pre-set voltage of contacts m is 1V, and contact k is of 0V, the impedance between m and k will be

$$Z_{mk} = \frac{1}{\int_{\Gamma_k} (\sigma + j\omega\varepsilon)E_n d\Gamma}. \tag{6}$$

where Γ_k is the surface of contact k. σ and ε are the conductivity (reciprocal of resistivity) and permittivity of the medium surrounding contact k, respectively.

Note that only E_n is needed in (6). This can be made use of later.

Now we start solving E_n from (3). Utilizing the Green's identities, and selecting free-space Green's function as weighting function, we transform (3) into a boundary integral equation (BIE), which is defined on the boundary of medium M_i. Partition the boundary into N_i elements Γ_{ij}. Then we get a discretized BIE [11]:

$$c_s u_s + \sum_{j=1}^{N_i} \int_{\Gamma_{ij}} q^*_{(s)} u d\Gamma = \sum_{j=1}^{N_i} \int_{\Gamma_{ij}} u^*_{(s)} E_n d\Gamma, \text{ for medium } M_i \tag{7}$$

where collocation point s is on the boundary of M_i. c_s is a constant. $u^*_{(s)}$ is the fundamental solution of Laplace equation which is related with point s, and $q^*_{(s)}$ is its normal derivative. Here, u^* is equal to the free-space Green's function.

List the equations (7) for each of the mediums in the substrate. Combine these equations with the interface conditions (5). Substitute the conditions (4), and we get an overall system

$$\boldsymbol{A}\boldsymbol{x} = \boldsymbol{b}, \tag{8}$$

where $\boldsymbol{A}$ is composed of complex entries. Vector $\boldsymbol{x}$ is constituted by u and E_n unknowns of all mediums. $\boldsymbol{b}$ is created after moving all the known values related to pre-set voltage $\overline{u}$ to the right side. Solving the system, we can directly get E_n, and in turn the impedance in (6). When the impedances between many pairs of contacts are desired, the system (8) will become

$$\boldsymbol{AX} = \boldsymbol{B}, \tag{9}$$

where $\boldsymbol{B}$ is also a matrix.

III. Effective Techniques for DBEM

Although DBEM has much fewer variables in some sense, it seems still too slow for substrates with many contacts. Accelerating techniques are preferred.

A. Reuse Matrix

To evaluate a lossy substrate, we usually need to calculate coupling impedances at many frequencies. Usually we need to build the system (9) for many times. However, most entries of matrix $\boldsymbol{A}$ and vector $\boldsymbol{B}$ can be reused so as to save the computational time.

For an interface element, there is a pair of variables $E_{n,a}$ and $E_{n,b}$ related to it. In medium a, the coefficient of $E_{n,a}$, denoted by I_a, can be determined by the integral in (7). In medium b, I_b, the coefficient of $E_{n,b}$ can be similarly obtained. $E_{n,a}$ and $E_{n,b}$ have the relationship of $E_{n,b} = \dfrac{\sigma_a + j\omega\varepsilon_a}{\sigma_\square + j\omega\varepsilon_\square} E_{n,a}$. Actually, to overcome the singularity of the matrix, we keep one of them in the system, say $E_{n,a}$. Then the $E_{n,a}$ coefficient in medium b becomes $I_b \times \dfrac{\sigma_a + j\omega\varepsilon_a}{\sigma_b + j\omega\varepsilon_b}$, which depends on ω.

In a word, only those matrix entries related to the interface variables like $E_{n,a}$ are frequency-dependent. The other entries remain the same for any frequency. Besides, $\boldsymbol{B}$ in (9) is also independent of frequency, because it is merely related to the pre-set voltage $\overline{u}$ and the integral similar to I_a.

When impedances at multiple frequencies are needed, we need to build the system (9) for each frequency as usual. However, a better choice is to compute the aforementioned frequency-independent entries only once, and reuse them for any frequency. The other entries are re-calculated at each frequency. In this way some CPU time can be saved. For the first test case in Section IV, this reusing technique reduces the total running time for 20 frequencies from 144.91 to 124.70 seconds, or by 14%.

B. Condense the Linear Equation System

Solving the complex system (9) consumes a great deal of CPU time. Direct solutions have too high computational complexity. As we will see in subsection *C*, the coefficient matrix is sparse for multi-medium problems, so we choose a GMRES solver [14]. Moreover, reordering unknowns and corresponding collocation points in the same sequence can make the matrix diagonally dominant [3]. Reorder unknowns as in Fig.2 can arrange non-zero blocks as close to the diagonal as possible [3, 12]. These can shorten solution time to some extent. But solving a large linear system takes still too much time.

However, if we discard inessential variables at first, and the consequent solving the condensed system will be much easier. Remind that only E_n variables are needed in (6), so we can discard some u variables. Rewrite a system $\boldsymbol{Ax} = \boldsymbol{b}$ in terms of sub-matrices (for (9), we can do it similarly):

$$\begin{bmatrix} \boldsymbol{A_{00}} & \boldsymbol{A_{0T}} \\ \boldsymbol{A_{T0}} & \boldsymbol{A_{TT}} \end{bmatrix} \cdot \begin{bmatrix} \overline{\boldsymbol{x}} \\ \boldsymbol{u_T} \end{bmatrix} = \begin{bmatrix} \boldsymbol{b_0} \\ \boldsymbol{b_T} \end{bmatrix}, \tag{10}$$

where $\overline{x}$ and $\boldsymbol{u_T}$ are two subsets of $\boldsymbol{x}$. Remove the inessential $\boldsymbol{u_T}$ equivalently:

$$\overline{\boldsymbol{A}}\,\overline{\boldsymbol{x}} = \overline{\boldsymbol{b}}, \tag{11}$$

where

$$\overline{\boldsymbol{A}} = \boldsymbol{A_{00}} - \boldsymbol{A_{0T}} \boldsymbol{A_{TT}^{-1}} \boldsymbol{A_{T0}}, \tag{12}$$

and

$$\overline{\boldsymbol{b}} = \boldsymbol{b_0} - \boldsymbol{A_{0T}} \boldsymbol{A_{TT}^{-1}} \boldsymbol{b_T}. \tag{13}$$

The condensing procedure (12) (13) is generally expensive in computation, because it involves the inversion of $\boldsymbol{A_{TT}}$ and matrix-matrix multiplications.

We start to reduce the computational complexity of (12) (13). For an example three-layer substrate, reordering the non-interface variable v_{33} of medium 3:

$$v_O \rightarrow E_{nC} \rightarrow u_T, \tag{14}$$

where E_{nC} represents the unknown E_n on contact surfaces, u_T denotes u unknowns on the top surface of medium 3, and v_O denotes the other unknowns in v_{33}.

With the ordering (14) and Fig.2 applied, the DBEM matrix $\boldsymbol{A}$ for a substrate is shown in Fig.3a, where zero entries are in white. The condensed matrix $\overline{A}$ is in Fig.3b. $\boldsymbol{A_{TT}}$ is diagonal; $\boldsymbol{A_{0T}}$ and $\boldsymbol{b_T}$ are sparse. These properties can be analytically proven. Refer to [3] for more details. Thus calculating $\overline{A}$ and $\overline{b}$ through (12) (13) is easier.

$$\begin{aligned} & v_{11} \rightarrow u_{12} \rightarrow u_{13} \rightarrow \ldots \rightarrow u_{1M} \\ & \rightarrow q_{21} \rightarrow v_{22} \rightarrow u_{23} \rightarrow \ldots \rightarrow u_{2M} \\ & \rightarrow q_{31} \rightarrow q_{32} \rightarrow v_{33} \rightarrow \ldots \rightarrow u_{3M} \\ & \rightarrow \ldots \ldots \ldots \ldots \ldots \ldots \ldots \ldots \ldots \\ & \rightarrow q_{M1} \rightarrow q_{M2} \rightarrow q_{M3} \rightarrow \ldots \rightarrow v_{MM} \end{aligned}$$

Fig. 2 Reorder unknowns. M is the number of mediums. v_{ii} includes u on Dirichlet boundary and q on Neumann boundary of medium i. u_{ij} and q_{ji} ($i < j$) are on the interface of mediums i and j.

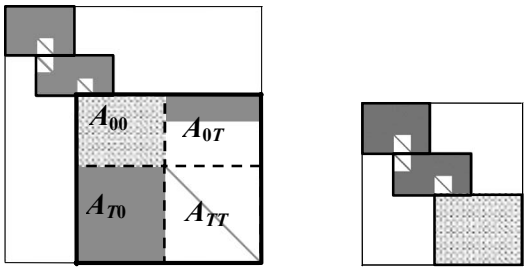

Fig. 3. Distribution of nonzero entries in $\boldsymbol{A}$: (a) original; (b) after using the condensing technique. Zero entries are in white.

In the first experiment in Section IV, it takes 4.1 seconds to solve (8). If the condensing technique is applied, the solution takes merely 1.5 seconds, or 60% is saved. Unfortunately, the condensing procedure (12) (13) itself takes 5.0 seconds. But when the sparsifying technique in the next subsection is applied, the procedure needs only 0.58 seconds.

On the other hand, there is only one right-hand side here. If there are many sides as (9) indicates, the condensing technique will bring higher efficiency [3, 11], since solution time for each side is considerably reduced.

C. Sparsify Matrix

From Fig.3, we learn that coefficient matrix $\boldsymbol{A}$ is blocked sparse. The sparsity can be analytically deduced from equation (7), where collocation points and variables related to each other are within the same medium. In other words, collocation points and variables in different mediums have no direct numerical relationship. Therefore, $\boldsymbol{A}$ is blocked sparse for multi-medium problems.

If a physical medium is quasi-cut into fictitious components, the matrix sparsity can be enlarged. This is the basic idea of a quasi-multiple medium (QMM) technique in [11, 12]. For an example substrate, if we cut the third medium into 6 smaller components, the original matrix Fig.4a turns into a sparser one Fig.4b. The new matrix is a bit larger, because the quasi-cutting will bring additional variables on interface of adjacent fictitious components. What's most important is the total number of non-zero entries is remarkably reduced. Since most time is spent in matrix-vector multiplication in a GMRES solver, the enhanced sparsity is certain to speed up the solution. Similarly, the technique can also speed up the condensing procedure (12) (13).

For instance, in the first experiment in Section IV, solution time of (9) is reduced from 4.1 seconds to 2.0 seconds, and the speed up is 2.

As we have seen, each of the three techniques above can enhance the efficiency of DBEM without any accuracy loss. What's more, if they are combined together, the enhancement will be more obvious, as shown in the next section.

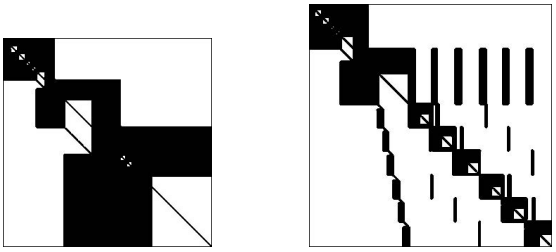

Fig. 4. (a) Original matrix, with 248,700 nonzero entries. (b) Matrix after the QMM idea is used, with 142,716 nonzero entries.

IV. Numerical results

The first experiment is a substrate involving a top contact and a back plane, as shown in Fig.5a. And the second case is shown in Fig.5b, involving a back plane and two top contacts separated by s μm. The test cases will be configured with two types of substrate processes [4], as shown in Fig.6. In order to be compatible with literature data, the contacts are assumed to be of zero heights.

For the first test case, the impedances obtained with the presented DBEM are depicted in Fig.7 (for the LR process) and Fig.8 (for the HR process), respectively. The data in [4] are also depicted. The figures indicate that with any process, the magnitude of impedance decreases as the frequency increases. This is because the substrate current injection is capacitive in nature [4]. With the low-resistivity (LR) process, the impedance is smaller in magnitude than with the high-resistivity (HR) process. This is because the bulk is with much smaller resistivity in the LR process.

Both the magnitude and the phase of the impedances obtained with DBEM are very close to literature data. The discrepancy is within 1.0%, which also includes the possible error of experiment setups (we did not find the exact setups in [4]). In a word, DBEM has a high accuracy.

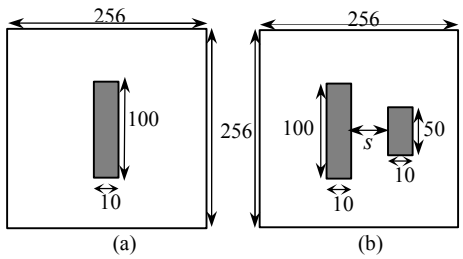

Fig. 5. (a) A single contact at center. (b) Two contacts located symmetrically along the center with distance of s μm. There is a back plane in the two substrates.

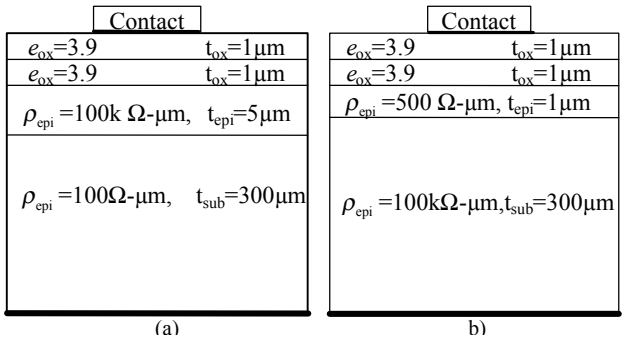

Fig. 6. Side views of two doping profiles [4]. (a) Low-resistivity (LR) process; b) high-resistivity (HR) process. Bottom bold lines denote back planes.

Take a look at the efficiency. Since running parameters of the method in [4] can not be obtained, we do not compare DBEM with it directly. But the superiority of DBEM over Green's function methods for substrate impedance modeling can be roughly deduced according to [3] and [11], where DBEM is up to hundreds of times faster than the excellent eigendecompostion method in [2] for resistance extraction.

The total running time to get the impedances at 20 frequencies is listed in Table 1. All DBEM programs run on a Sun Fire 880 workstation, with CPU frequency of 750 MHz. The table tells us that each of the techniques in section III can bring enhancement of efficiency. Furthermore, their combination performs much better, with a speed-up of 2.7 over pure DBEM.

For the two-contact substrate Fig.5b, the contact-contact impedance depends on the spatial separation. The impedance of this substrate with the LR process is depicted in Fig. 9. We learn that the impedance is very sensitive to the distance *s*. As *s* extends from 2μm to 10μm, the impedance increases by three times in magnitude. When *s* turns from 10μm to 50μm, the impedance rises by ten times. The same tendency is found in [4].

Note that the both doping profiles in Fig. 6 are stratified. However, these methods based on Green's functions have

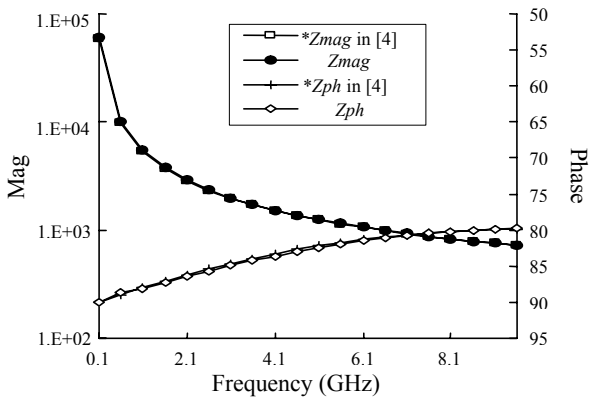

Fig. 7. Magnitude and phase of the contact-ground impedance of the single-contact substrate with the LR process.

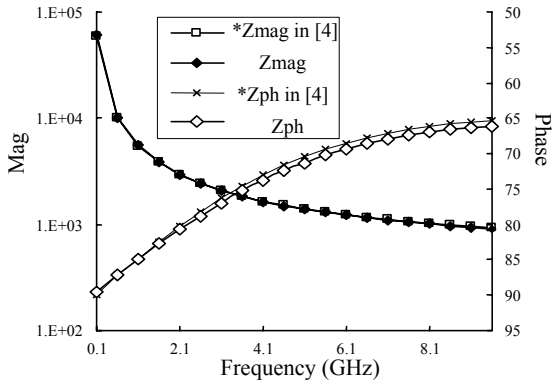

Fig. 8. Magnitude and phase of the contact-ground impedance of the single-contact substrate with the HR process.

much difficulty in handling substrates with non-stratified doping profiles. In reality, there are many such substrates. For example, there are many lateral variation components in the substrates, such as oxide trenches and wells [9]. In order to illustrate the versatility of DBEM, examine the simple example shown in Fig. 10, where the top central block in gray has a distinct resistivity from its lateral neighbor. We call the block "LVB" (lateral variation block).

TABLE I.
Running time for substrate Fig.5a with LR process

Pure DBEM	**144.91**
DBEM + Reusing (Sect III.A)	124.70
DBEM + Condensing (Sect III.B)	74.06
DBEM + Sparsifying (Sect III.C)	70.54
DBEM+Reusing+Condensing+Sparsifying	**52.90**

Since the conductivity of epi layer (2000 s/m) is large, and at frequency of up to 10 GHz, the ohmic current is dominant over the displacement current in the layer. Thus changing the dimension of the higher-resistivity LVB block will have limited impact on the contact-contact impedance, as shown in Fig. 11.

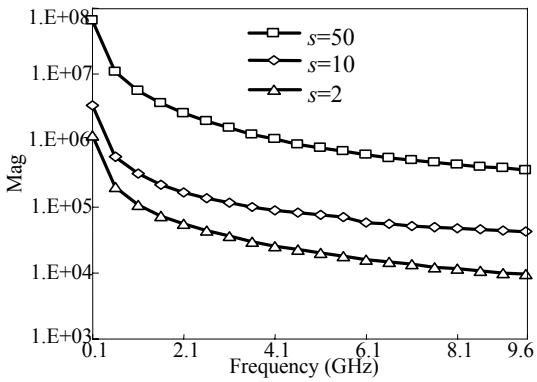

Fig. 9. Magnitude of the contact-contact impedance of the two-contact substrate Fig. 5b, with the LR process. *s* is the distance between the contacts.

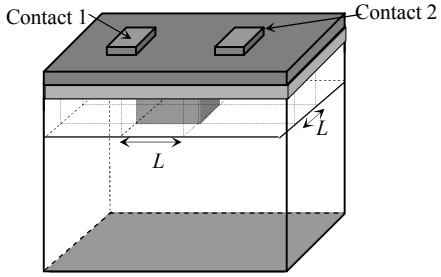

Fig. 10. Substrate with lateral resistivity variation in the epi layer of the HR process. The width and length of the substrate are 200 μm. The resistivity of the epi layer and the gray block are 5e-4 and 0.5 Ωm, repectively. Note that each contact here is modeled as a block with 3-D shape, as well as the LVB block.

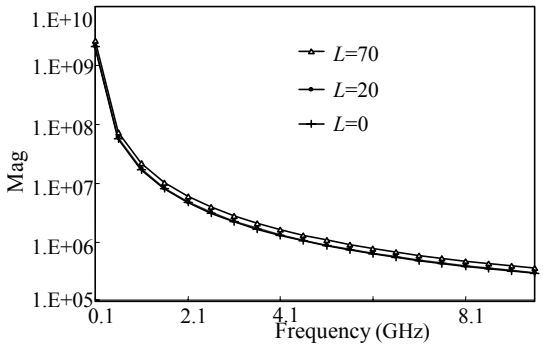

Fig. 11. Magnitude of the contact-contact impedance. Since the epi layer of HR process is very small, the central block is not possible to be large, and thus the curves are close to each other.

Fig.11 illustrates that when the LVB block is small (L=0, or L=20), the impedance is relatively small. As the block grows large (L=70), the impedance increases, since it obstructs the ohmic current flow considerably. Besides, for a specified frequency, the difference between the impedances under different L is small. A reason is that the obstructing LVB block can not be very large due to spatial limitation.

The results tell us that DBEM is able to simulate such complex substrates without any difficulty.

Note that the accuracy of DBEM can be further improved by partitioning the substrate boundary more densely. On the other hand, the efficiency of it may also be enhanced by partitioning more coarsely. This allows a tradeoff of them, which makes the method adaptive in various circumstances.

V. Conclusions

In this paper, we present a new direct boundary element method (DBEM) to extract the impedances of lossy substrates at any frequency. Based on Maxwell equations, we deduce the Laplace equation that holds in the substrate and its boundary conditions. Utilizing the complex current continuity conditions on the interfaces of lossy mediums, the new DBEM becomes suitable for impedance modeling. Three accelerating techniques are proposed without any sacrifice of accuracy. Reusing matrix entries can save lots of time for building matrices for impedance extraction at multiple frequencies. Condensing the linear system and sparsifying the coefficient matrix can speed up system solution remarkably. Numerical experiments illustrate that DBEM can be of high accuracy and high efficiency. DBEM is able to simulate substrates with arbitrarily processes, and numerical experiment results are reasonable.

References

[1] R. Gharpurey and E. Charbon, "Substrate coupling: Modeling, simulation and design perspectives," *Proc. 5th International Symposium on Quality Electronic Design*, pp. 283-290, 2004.

[2] J.P. Costa, M. Chou, and L.M. Silveira, "Efficient techniques for accurate modeling and simulation of substrate coupling in mixed-signal IC's," *IEEE Trans. Comput. Aided Design*, Vol. 18, pp. 597-607, 1999.

[3] X. Wang, W. Yu, and Z. Wang, "Substrate Resistance Extraction with Direct Boundary Element Method," *Asia and South Pacific Design Automation Conference*, pp.208-211, 2005.

[4] A.M. Niknejad, R. Gharpurey, and R.G. Meyer, "Numerically stable Green function for modeling and analysis of substrate coupling in integrated circuits," *IEEE Trans. Comput. Aided Design*, Vol. 17, pp. 305-315, 1998.

[5] N.K. Verghese and D.J. Allstot, "Fast simulation of substrate coupling effects in mixed-mode ICs," *IEEE Custom Integrated Circuits Conference*, pp. 18.3.1–18.3.4, 1993.

[6] T. Smedes, N.P. van der Meijs, and A.J. van Genderen, "Extraction of circuit models for substrate cross-talks," *IEEE/ACM International Conference on Computer-Aided Design*, pp. 199-206, 1995.

[7] R. Ghapurey and R.G. Meyer, "Analysis and simulation of substrate coupling in integrated circuits," *International Journal of Circuit Theory and Application*, Vol. 23, pp. 381–394, 1995.

[8] C. Xu, T. Fiez and K. Mayaram, "On the numerical stability of Green's function for substrate coupling in integrated circuits," *IEEE Trans. Computer-Aided Design*, Vol. 24, pp. 653–658, 2005.

[9] S. Donnay and G. Gielen, *Substrate Noise Coupling in Mixed-Signal ASICs*. Kluwer Academic Publishers, 2003.

[10] S. Ardalan and M. Sachdev, "An overview of substrate noise reduction technieques," *Proc. 5th International Symposium on Quality Electronic Design*, pp. 291-296, 2004.

[11] X. Wang, W. Yu, Z. Wang, and X. Hong, "An improved direct boundary element method for substrate coupling resistance extraction," *Proceedings of the ACM Great Lakes Symposium on VLSI* , pp. 84-87, 2005.

[12] W. Yu, Z. Wang, and J. Gu, "Fast capacitance extraction of actual 3-D VLSI interconnects using quasi-multiple medium accelerated BEM," *IEEE Trans. Microwave Theory Tech.*, Vol. 51, pp. 109-199, 2003.

[13] S. Ramo, J.R. Whinnery, and T. van Duzer, *Fields and Waves in Communication Electronics,* 2nd ed. New York: Wiley, pp. 279-283, pp. 572-676, 1984.

[14] Y. Saad and M.H. Schultz, "GMRES: A generalized minimal residual algorithm for solving nonsymmetric linear systems," *SIAM J. Sci. Statis. Comput.*, Vol. 7, pp. 856-869, 1986.

[15] S. Ramo, J.R. Whinnery, and T. van Duzer, *Fields and Waves in Communication Electronics,* 3rd ed. New York: Wiley, pp. 283-287, pp. 572-676, 1994.